aerospace

MDPI

Article

Study on Flow Field Characteristics of High-Speed Double-Row Ball Bearings with Under-Race Lubrication

Xiaozhou Hu * and Jian Lin

School of Mechanical and Electrical Engineering, Central South University, Changsha 410083, China; 13600845973@163.com

* Correspondence: huxiaozhou@csu.edu.cn

Abstract

As a core component of aero-engines, double-row ball bearings' lubrication performance directly impacts the operational stability of the aircraft engine. However, existing under-race lubrication designs primarily rely on empirical knowledge, with insufficient understanding of the complex oil–air two-phase flow mechanisms, leading to bottlenecks in optimizing lubrication efficiency. Therefore, based on the computational fluid dynamics (CFD) method, a two-phase flow model for double-row ball bearings was established to systematically analyze the influence patterns of key parameters—including rotational speed, oil supply rate, number of under-race holes, diameter of under-race holes, and oil properties (viscosity, density)—on the distribution of the oil–air two-phase flow. The findings reveal that (1) the oil in the circumferential direction of the bearing cavity exhibits periodic distribution characteristics correlated with the number of under-race holes; (2) the self-rotation effect of balls hinders the migration of oil toward the outer raceway region, resulting in a significant reduction in the oil volume fraction within the bearing cavity; (3) compared with the single-sided oil supply configuration, the double-sided oil supply structure demonstrates superior lubrication performance. These research results provide theoretical support and reference data for the optimal design of under-race lubrication systems for double-row ball bearings.

Keywords: double-row ball bearing; under-race lubrication; self-rotation of balls; oil distribution; aero-engine

check for updates

Academic Editors: Yang Zhang and Kung-Ming Chung

Received: 26 July 2025
Revised: 17 September 2025
Accepted: 23 September 2025
Published: 24 September 2025

Citation: Hu, X.; Lin, J. Study on Flow Field Characteristics of High-Speed Double-Row Ball Bearings with Under-Race Lubrication. *Aerospace* **2025**, *12*, 861. https://doi.org/10.3390/aerospace12100861

Correction Statement: This article has been republished with a minor change. The change does not affect the scientific content of the article and further details are available within the backmatter of the website version of this article.

Copyright: © 2025 by the authors. Licensee MDPI, Basel, Switzerland. This article is an open access article distributed under the terms and conditions of the Creative Commons Attribution (CC BY) license (https://creativecommons.org/licenses/by/4.0/).

1. Introduction

The development of aero-engines is advancing toward high power, high rotational speeds, and elevated thrust-to-weight ratios. In the design and performance evaluation of aero-engine main shaft bearings, the diameter–nominal speed value (DN value) is a critical parameter central to both the design process and performance assessment. Currently, the DN value (rotational speed (rpm) × inner diameter (mm)) of aero-engine main shaft bearings continues to rise, with DN values of some bearings in high-performance engines exceeding 3×10^6 [1]. As core components of aero-engines, double-row ball bearings operate continuously under extreme conditions including high speeds, elevated pressures, intense heat, and heavy loads. Their lubrication performance is crucial for ensuring engine operational stability [2]. The resultant frictional heat generation increases exponentially at high speeds, presenting significant challenges to bearing lubrication and cooling. Inadequate lubrication compromises effective heat dissipation, leading to thermal accumulation within the bearing chamber [3]. This buildup causes chamber overheating, oil coking, and

severe degradation or damage to bearings. Consequently, engine vibration may ensue, potentially triggering catastrophic events such as shaft seizure. Therefore, comprehensive investigation into lubricant flow dynamics within bearings is essential for optimizing lubrication and cooling strategies to maintain engine reliability.

Common lubrication methods for bearings include jet lubrication, oil–air lubrication, and oil–mist lubrication [4], with jet lubrication being extensively employed in aero-engines. However, for bearings with high DN values, high-velocity airflow within the bearing cavity creates high-pressure zones that atomize and break up injected oil [5]. This impedes lubricant ingress into the bearing chamber, substantially reducing lubrication efficiency. To address inadequate lubrication efficiency in main shaft bearings with high DN values, researchers have proposed under-race lubrication. By incorporating radial holes and oil grooves in the bearing inner ring, this method delivers oil directly into the bearing cavity. Centrifugal forces enable the oil to penetrate the high-pressure zones generated by rapid airflow and propel it toward the outer ring, achieving efficient cooling and lubrication. Compared with jet lubrication, under-race lubrication demonstrates superior performance through reduced oil consumption, more precise delivery to targeted regions, and enhanced cooling and lubrication effectiveness [6].

The complex motion within high-speed rolling bearings results in intricate oil–air two-phase flow in bearing cavities. Meanwhile, since the heat generation and heat transfer coupling of bearings are often influenced by the flow characteristics of two-phase flow, and the temperature field in the bearing cavity largely depends on the oil volume fraction within the cavity [7], it is necessary to conduct research on the oil–air two-phase flow within the bearing cavity to understand its flow characteristics. Extensive research is conducted on bearing lubrication: Peterson et al. [8] established full-scale deep-groove bearing models to investigate rolling element number, lubricant viscosity, inner race speed, and cage design effects on two-phase flow. Drawing upon the CFD approach integrated with the VOF two-phase model and sliding mesh methodology, Wu et al. [4,9] investigated oil–air two-phase flow in jet-lubricated ball bearings. Their analysis quantified the effects of rotational speed, lubrication supply parameters, and nozzle configuration on internal oil volume fraction. Yan et al. [10] established numerical models for bearings with various nozzle distributions. Through CFD simulations incorporating self-rotation of balls and contact angle influences under diverse sealing conditions, they comprehensively evaluated temperature and pressure distributions, airflow patterns, and oil volume fraction. Findings revealed that sealing structures significantly enhance lubricant delivery to contact interfaces. To address the insufficient lubricant distribution problem in conventional cage designs, Qian et al. [11] proposed cages with diverter holes. CFD comparisons confirmed enhanced oil volume fraction within bearing cavities using modified cages, leading to significantly improved contact zone lubrication. Dai et al. [12] computationally investigated two-phase flow dynamics in high-speed angular contact ball bearings, experimentally validating “oil penetration rate” as a key lubrication metric. Their study elucidated how operational (speed, oil flow) and geometric (roller count) parameters influence penetration performance, establishing robust agreement between CFD and experimental data. The developed physical model provides a reliable foundation for parametric performance evaluation of bearing two-phase flows.

For under-race lubrication of single-row bearings, some scholars have already conducted research on the two-phase flow field and temperature field within the bearing cavity. In terms of research on the flow field inside the bearing cavity, Adeniyi et al. [13] numerically demonstrated that after exiting under-race supply holes, lubricant adheres to the inner race surface before being centrifugally propelled onto cages. Oil subsequently separates from cage sidewalls to enter the primary bearing flow domain. Research by Gao [14] revealed a non-monotonic relationship: increasing oil supply or inlet velocity

initially enhances then reduces the average oil volume fraction. Optimal values exist that maximize lubricant retention within bearing cavities while accounting for self-rotation of balls effects. Adeniyi et al. [15] employed the CLSVOF method to simulate two-phase flow in aero-engine under-race lubricated ball bearings. Their work characterized oil droplet transport while accounting for load, contact angle, and ball rotational dynamics, though neglecting elastohydrodynamic lubrication (EHL) effects on pressure and viscosity. Yu et al. [16] numerically assessed the influence of rotational speed, oil flow rate, viscosity, and density of lubricating oil on oil distribution at inner and outer raceway contact zones, identifying distinct periodic distribution patterns. Gong et al. [17] explored structural parameter impacts on two-phase flow characteristics. Analysis of oil transport across varying cage clearances demonstrated that increased radial operating clearance and chamber clearance effectively improve lubrication performance. In terms of research on the temperature field within the bearing cavity, Wei et al. [18] developed a numerical model for the oil–air two-phase flow in the entire bearing under oil–mist lubrication. By considering the rotation and revolution of the balls, validating the model through visualization experiments, and analyzing the effects of oil temperature, oil type, and rotational speed on the two-phase flow, they revealed the following oil distribution patterns: the oil volume fraction in the outer ring is the highest, and the volume fraction in each part decreases with increasing rotational speed or oil temperature, thus providing theoretical support for the lubrication design of high-speed bearings. Bao et al. [19] developed a simplified 3D heat transfer model incorporating the Coupled Level Set and Volume of Fluid (CLSVOF) method for two-phase tracking and Palmgren's approach for heat generation, analyzing rotational speed and inlet velocity effects on oil volume fraction, temperature distributions, and convective heat transfer coefficients. Bao et al. [20] employed CFD simulation and experimental validation to investigate the effect of annular grooves on the inner ring temperature of star gear bearings with under-race lubrication. The results showed that annular grooves can significantly reduce the inner ring temperature, demonstrating the effectiveness of the optimized design.

However, there have been no systematic studies on the under-race lubrication of double-row ball bearings to date, with only a few scholars having investigated the lubrication of double-row tapered roller bearings. Zhu et al. [21] compared the outer ring rib and inner ring rib structures of double-row tapered roller bearings, analyzing the lubrication performance under full lubrication and oil starvation conditions through experiments and CFD simulations. The results showed that the outer ring rib structure exhibits superior lubrication performance and stronger dry running capability. Bai et al. [22], based on CFD and the discrete oil quantity method (R10 method), analyzed the lubricant distribution of double-row tapered roller bearings under lubrication failure conditions. They found that the optimal rotational speed ranges from 4000 to 5000 r/min, providing a basis for the bearing design of helicopter tail drive systems.

In summary, current research on bearing lubrication predominantly focuses on jet lubrication systems, with inadequate attention directed toward oil–air two-phase flow characteristics in under-race lubricated ball bearings. Existing studies have exclusively examined single-row bearings, leaving double-row ball bearings under under-race lubrication entirely unexplored. The structural complexity of double-row bearings—featuring two independent raceways and ball sets—results in mutual interference between their rotational motions, significantly complicating internal oil transport. Consequently, investigating oil flow behavior in under-race lubricated double-row bearings is essential for advancing thermal transfer understanding and enabling refined lubrication design optimization. This study innovatively investigates the flow characteristics of oil–air two-phase flow inside double-row ball bearings with under-race lubrication, and analyzes the effects of operational variables (rotational speed, oil supply rate), structural parameters (number

and diameter of under-race holes), and oil properties (viscosity, density) on internal oil distribution. Particular focus addresses how self-rotation of balls and the positions of under-race holes influence oil distribution within the bearing cavity and across raceway interfaces. However, it is worth noting that this study focuses on the macroscopic flow field characteristics of the bearing cavity rather than the microscopic flow field level; therefore, the research on bearing heat generation and temperature field is not considered for now.

2. Model and Method

2.1. Geometric Model

Compared to single-row angular contact bearings, double-row angular contact bearings exhibit superior overall rigidity, higher load-carrying capacity, and more compact structure. They deliver enhanced reliability under high rotational speeds, heavy loads, and harsh operating conditions, thus being extensively employed on aircraft engine main shafts—as exemplified by Bearing No.3 in Figure 1. To investigate oil–air two-phase flow characteristics in under-race lubricated double-row ball bearings, a simplified bearing model is established, as shown in Figure 2. The model comprises an inner ring, outer ring, cage, and balls, with under-race lubrication holes uniformly distributed around the inner race circumference. Driven by centrifugal forces, oil enters the bearing interior through these holes and subsequently exits via both axial ends. Key geometric parameters of the double-row bearing are detailed in Table 1. Reflecting practical configurations where double-row bearings operate under preloaded conditions, zero radial clearance exists between balls and raceways. For computational feasibility, a 0.3 mm clearance is implemented between rolling elements and raceways—an established simplification methodology widely adopted in bearing lubrication simulations [23]. Throughout all simulations, the outer ring remains stationary while rotational motion is specifically applied to the inner ring (representing the bearing rotational speed).

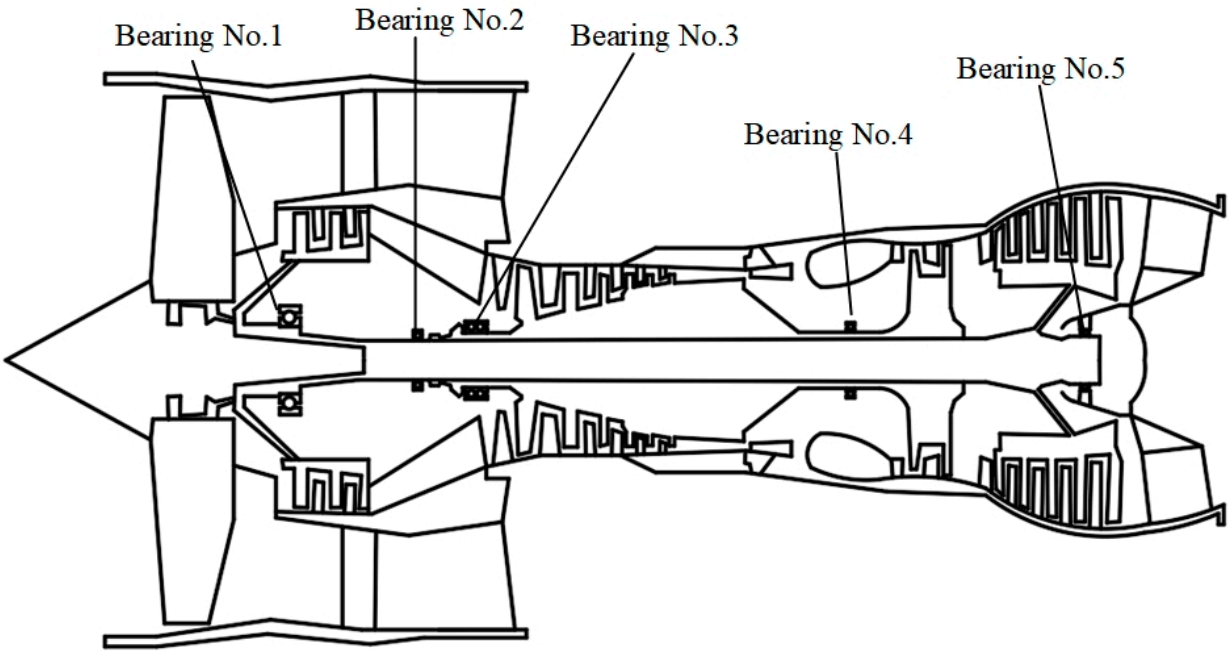


Figure 1. Schematic diagram of aero-engine structure.

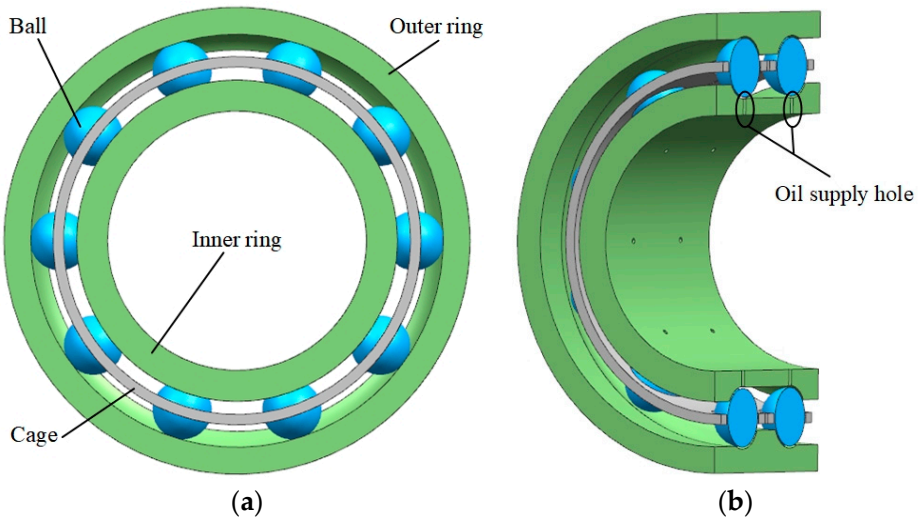


Figure 2. Double-row angular contact bearing with under-race lubrication: (**a**) overall view of bearing; (**b**) bearing sectional view.

Table 1. Geometry parameters of double-row angular contact bearing.

Geometry Parameters	Specification
Inner ring diameter (mm)	50
Bearing width (mm)	40
Pitch diameter (mm)	68.5
Contact angle (°)	30
Ball diameter (mm)	12.3
Ball number	20

2.2. Meshing of Fluid Domain

The present study focuses exclusively on internal oil–air two-phase flow characteristics in double-row ball bearings. Consequently, the simulation model retains only the fluid domain, excluding the solid bearing components, which comprises three distinct regions: main flow region, stationary region, and under-race oil supply holes region, as shown in Figure 3. Conventional numerical simulations often inadequately define flow boundaries at geometric peripheries, disregarding cavity-induced flow modulation effects on internal two-phase transport. To break through this limitation, stationary region flanking the main flow region is incorporated to accurately represent cavity influences while substantially mitigating end-wall reflux artifacts. The oil supply holes region features two annular arrays totaling 16 uniformly distributed holes circumferentially arranged along the inner ring. The oil supply holes region rotates concentrically with the bearing center at the inner ring rotational speed n. The main flow zone velocity is equated to the cage orbital speed, which corresponds to the motion of the balls. The orbital speed n_b of the cage is

$$n_b = \frac{1}{2} n\left(1 - \frac{D_b \cos \alpha}{d}\right) \tag{1}$$

where n_b represents the ball orbital speed (rpm), n denotes the inner ring rotational speed (rpm), D_b signifies the ball diameter (mm), α indicates the contact angle (°), and d is the bearing pitch diameter (mm).

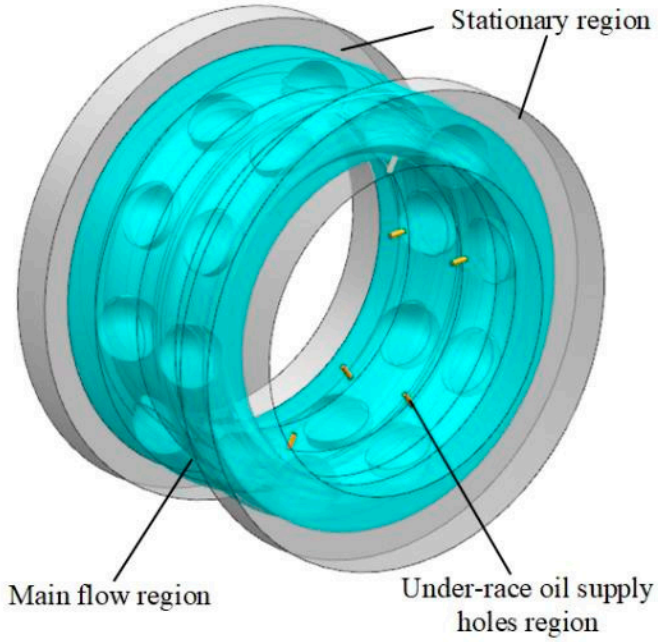


Figure 3. Computational domain of bearing.

The ball exhibits the most complex kinematic behavior among bearing components, simultaneously undergoing orbital rotation about the bearing axis at velocity n_b and spinning about its own axis at rotational speed n_s. Assuming no sliding occurs between the balls and raceways, the self-rotation velocity is expressed as

$$n_s = -\frac{1}{2}n\left(\frac{d}{D_b} - \frac{D_b \cos^2 \alpha}{d}\right) \quad (2)$$

The computational fluid domain is meshed using ANSYS2022R1 Meshing software. Given the complex internal structure of the bearing and the small clearances between the balls and the inner and outer raceways as well as the cage pockets, unstructured tetrahedral elements are employed to discretize the main flow region. Structured hexahedral grids are applied to the stationary region and the under-race oil supply holes region. This hybrid approach combining hexahedral and tetrahedral meshes effectively minimized the total cell number while ensuring simulation accuracy, thereby improving computational efficiency [12,24]. Mesh refinement is applied to the contact zones between the balls and cage pockets, inner/outer raceways, as well as the areas surrounding under-race oil supply holes to enhance mesh quality, as illustrated in Figure 4. Grid independence verification is conducted to ensure the reliability of simulation results, with corresponding data presented in Table 2, which demonstrate that increasing the mesh number beyond a specific threshold has negligible impact on the computational results. Considering both computational precision and efficiency, the final fluid domain model is discretized with a mesh configuration containing 3,209,238 elements and 766,531 nodes.

Table 2. Mesh independence verification.

Mesh Element Numbers	Difference in Flow Between Inlet and Outlet
1,816,758	5.83%
3,209,238	2.46%
4,028,005	2.38%

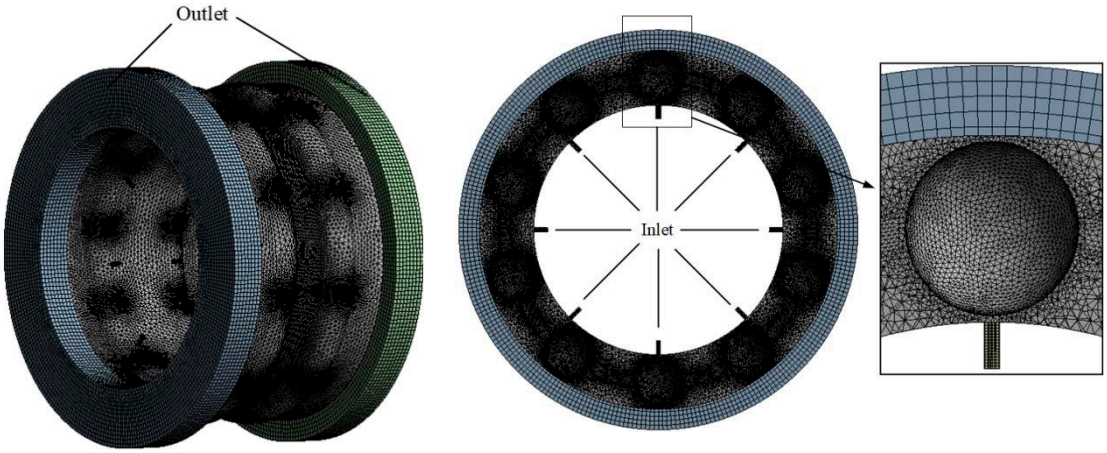


Figure 4. Mesh model.

The under-race oil supply holes machined in the inner ring are defined as mass flow inlets, while both terminal surfaces of the stationary region are set as pressure outlets at standard atmospheric pressure. A sliding mesh technique is implemented to simulate the relative rotational motion among the inner ring, balls, and cage. Data exchange between different bearing regions is facilitated through interface zones. The standard wall function is employed in the near-wall regions, with no-slip boundary conditions applied at all solid surfaces; specific boundary conditions are listed in Table 3.

Table 3. Boundary conditions.

Name	Type
Inner raceway	Moving wall, no-slip
Outer raceway	Stationary wall, no-slip
Ball	Moving wall, no-slip
Cage	Moving wall, no-slip
Inlet	Mass-flow inlet

2.3. Two-Phase Flow Model

The double-row ball bearing investigated in this study operates with under-race lubrication, where oil and air coexist within the bearing interior. The rotational motion of rolling elements and the cage generates a complex two-phase flow field within the assembly [25]. To accurately capture the oil–air interface, this paper employs the Volume of Fluid (VOF) model to characterize the interface between two immiscible fluids. The VOF model assumes that both the oil and air phases exist as continuous media coexisting within the computational domain. It utilizes a volume fraction function to represent both the free surface interfaces between different fluids and their respective volume proportions, while consistently maintaining their relative ratios. For any given control volume at any time instance, this relationship is defined as follows:

$$\varphi_{oil} + \varphi_{air} = 1 \tag{3}$$

where φ_{oil} and φ_{air} denote the volume fractions of oil and air, respectively.

It can be solved using the following volume fraction equation:

$$\frac{\partial}{\partial t}(\varphi_{oil}\rho_{oil}) + \nabla(\varphi_{oil}\rho_{oil}u_{oil}) = S_{\alpha_{oil}} + (\dot{m}_{oa} - \dot{m}_{ao}) \tag{4}$$

where ρ_{oil} is the oil density; $\dot{m}_{oa}$ is the mass transfer rate from the oil phase to the air phase per unit volume; $\dot{m}_{ao}$ is the mass transfer rate from the air phase to the oil phase per unit volume; $S_{\alpha_{oil}}$ is the generalized source term of the volume fraction equation.

The equivalent density and viscosity of the oil–air two-phase can be expressed as

$$\rho = \varphi_{oil}\rho_{oil} + (1 - \varphi_{oil})\rho_{air} \tag{5}$$

$$\mu = \varphi_{oil}\mu_{oil} + (1 - \varphi_{oil})\mu_{air} \tag{6}$$

2.4. Turbulence Model

When operating at high rotational speeds, significant differential speeds occur among bearing components, resulting in complex turbulent flow of the oil–air mixture within the bearing. Compared to conventional models, the Renormalization Group $k - \varepsilon$ model (RNG $k - \varepsilon$) incorporates modified coefficients in the dissipation rate transport equation, substantially enhancing its predictive capability for rapid strain and rotational flows. This advancement enables more accurate resolution of complex flow patterns arising from rotational motions of bearing components. Therefore, the RNG $k - \varepsilon$ model is selected for the present numerical simulation.

The turbulence kinetic energy (k) equation and turbulence dissipation rate (ε) equation of the RNG $k - \varepsilon$ model are, respectively, given as follows:

$$\frac{\partial(\rho k)}{\partial t} + \frac{\partial(\rho k u_i)}{\partial x_i} = \frac{\partial}{\partial x_j}[(\alpha_k \mu_{eff})\frac{\partial k}{\partial x_j}] + G_k + G_b - \rho\varepsilon - Y_M \tag{7}$$

$$\frac{\partial(\rho \varepsilon)}{\partial t} + \frac{\partial(\rho \varepsilon u_i)}{\partial x_i} = \frac{\partial}{\partial x_j}[(\alpha_\varepsilon \mu_{eff})\frac{\partial \varepsilon}{\partial x_j}] + C_{1\varepsilon}\frac{\varepsilon}{k}[(G_k + C_{3\varepsilon}G_b)] - C_{2\varepsilon}\rho\frac{\varepsilon^2}{k} - R_\varepsilon \tag{8}$$

The effective viscosity u_{eff} in this equation is determined by

$$\begin{cases} \mu_{eff} = \mu + \mu_t \\ \mu_t = \rho C_\mu \frac{k^2}{\varepsilon} \end{cases} \tag{9}$$

where G_k represents the turbulent kinetic energy production due to mean velocity gradients, G_b denotes the turbulent kinetic energy generation from buoyancy effects, YM quantifies the compressible turbulence dilation dissipation contribution, and α_k and α_ε are the inverse effective Prandtl numbers for turbulent kinetic energy and dissipation rate, respectively, governing turbulent diffusion.

2.5. Numerical Method

The numerical simulation of oil–air two-phase flow in the under-race lubrication system of a double-row ball bearing is conducted using ANSYS Fluent. A sliding mesh approach is applied to simulate rotational motions among distinct bearing regions. At initialization, the computational domain is entirely filled with air, setting the air volume fraction to unity and lubricant volume fraction to zero. Air is designated as the primary incompressible phase, with oil as the secondary phase. The lubricant is specified as Aeroshell Fluid 4109 with density 970 kg/m^3, while air has 1.225 kg/m^3. The dynamic viscosities are 0.0318 Pa·s and 1.7894×10^{-5} Pa·s, respectively. Governing equations are discretized using the finite volume method. Diffusion and pressure terms in the momentum equations employ central differencing, while convective terms use the second-order upwind PRESTO! (PREssure STaggering Option) scheme. Pressure–velocity coupling is resolved through the coupled algorithm. Convergence is determined through dual criteria: (1) monitoring solution residuals with energy, turbulent kinetic energy, and dissipation rate

residuals set to 10^{-3}, and other residuals to 10^{-5}; (2) tracking the net mass flux difference between inlet and outlets, requiring imbalance below 3% of the inlet mass flow rate. The solution is considered converged only when both conditions are simultaneously satisfied via the residual monitoring panel.

2.6. Validation of Simulation Methods

To validate the feasibility of the proposed numerical methodology, a computational model identical to the under-race lubrication configuration documented in Reference [26] is established. Parametric conditions from the reference are presented: an oil supply rate of 3 L/min, dynamic viscosity of 0.0046 Pa·s, and oil density of 938.6 kg/m^3. Comparative analysis focused on the average oil volume fraction within the bearing interior at various rotational speeds. As detailed in Table 4, numerical results obtained under identical operating conditions exhibit strong agreement with reference data, demonstrating a maximum relative deviation of merely 1.82%. This close correspondence validates the reliability of the present numerical approach for subsequent investigations.

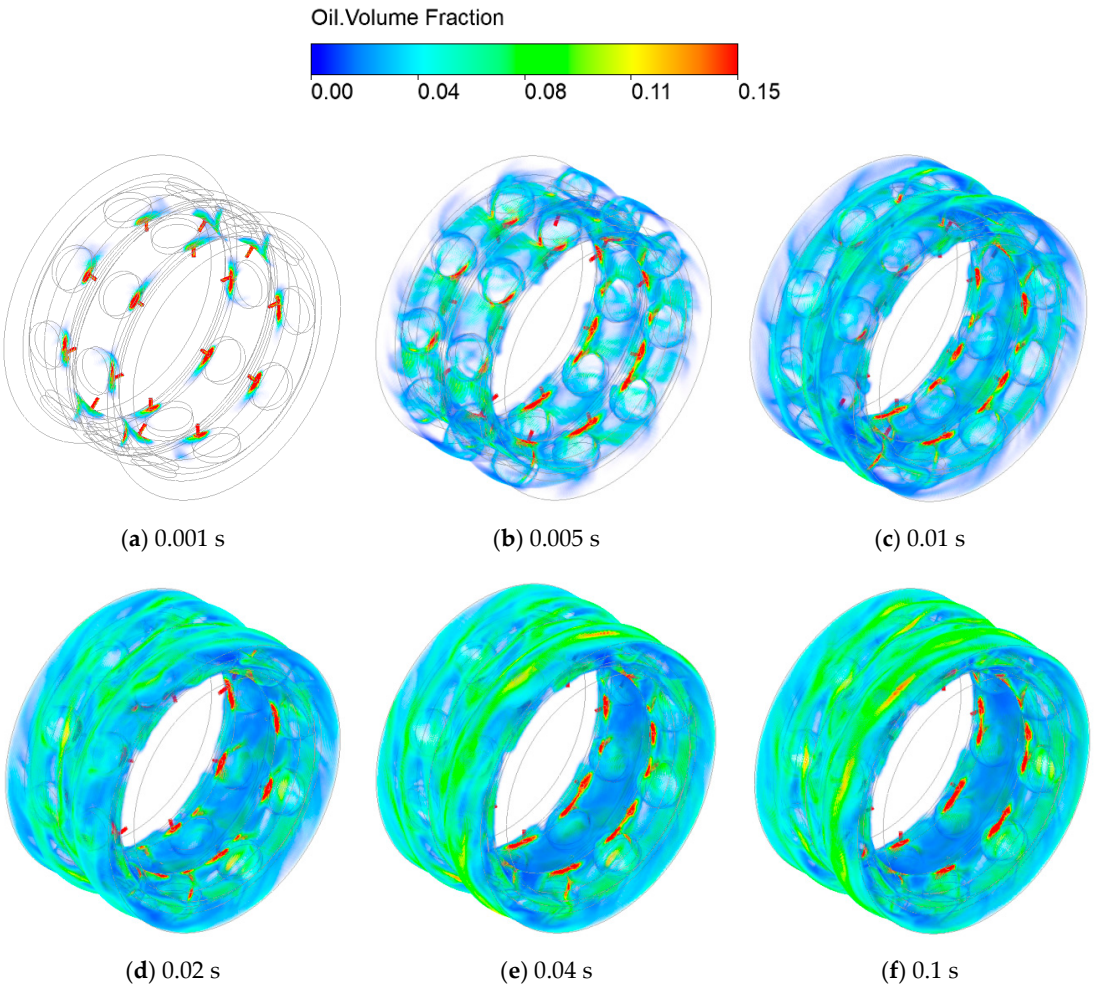
Table 4. Comparisons of the bearing cavity average oil volume fraction from simulation and literature.

Rotational Speeds (rpm)	Literature Oil Volume Fraction	Simulation Oil Volume Fraction	Relative Error
5000	0.01335	0.01323	0.90%
8000	0.00954	0.00963	0.94%
11,000	0.00748	0.00736	1.60%
14,000	0.00563	0.00557	1.07%
17,000	0.00439	0.00447	1.82%

3. Results and Discussion

3.1. Dynamic Characteristics of Oil–Air Two-Phase Inside the Bearing

The transient oil–air distribution within the bearing cavity at different time instances is presented in Figure 5. Simulations are conducted under the following conditions: inner ring rotational speed of 10,000 rpm (counterclockwise), inlet mass flow rate of 0.08 kg/s, under-race oil supply holes of 1 mm diameter arranged in two circumferential rows with eight holes per row, with a double-sided oil supply configuration implemented. Figure 5 demonstrates progressive oil accumulation within the bearing cavity. The oil volume fraction continuously increases during the initial stage, reaching quasi-steady distribution after 0.04 s when the average volume fraction stabilizes. Upon ejection from under-race holes, oil undergoes centrifugal acceleration away from the rotating inner ring. Upon momentary breakup through collisions with balls and cage components, a fraction of oil traverses cage pocket–ball clearances to reach the outer ring, forming a uniform circumferential coating on its stationary surface. Consequently, significantly higher oil concentration is observed near the outer raceway surface. Notably, uneven oil distribution occurs along the inner raceway, showing localized accumulation near supply holes, a phenomenon analogous to jet-lubricated ball bearings [9]. This flow pattern emerges primarily due to rotational transport mechanisms: centrifugal forces from inner ring rotation combine with rolling element trajectories to establish dominant circumferential oil transport pathways along the raceways.

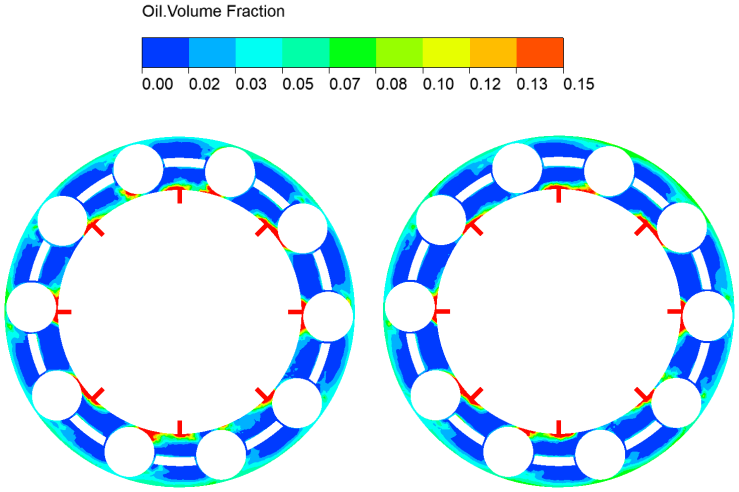


(**a**) 0.001 s (**b**) 0.005 s (**c**) 0.01 s

(**d**) 0.02 s (**e**) 0.04 s (**f**) 0.1 s

Figure 5. Oil distribution evolution inside the bearing cavity with flow time.

Figure 6 displays oil distribution contour plots on cross-sections of double-sided chambers in the double-row ball bearing. These contours reveal symmetrical lubricant distributions between left and right chambers. Oil accumulates primarily within two critical regions: adjacent to the outer raceway surface and surrounding the inner ring's oil supply holes.



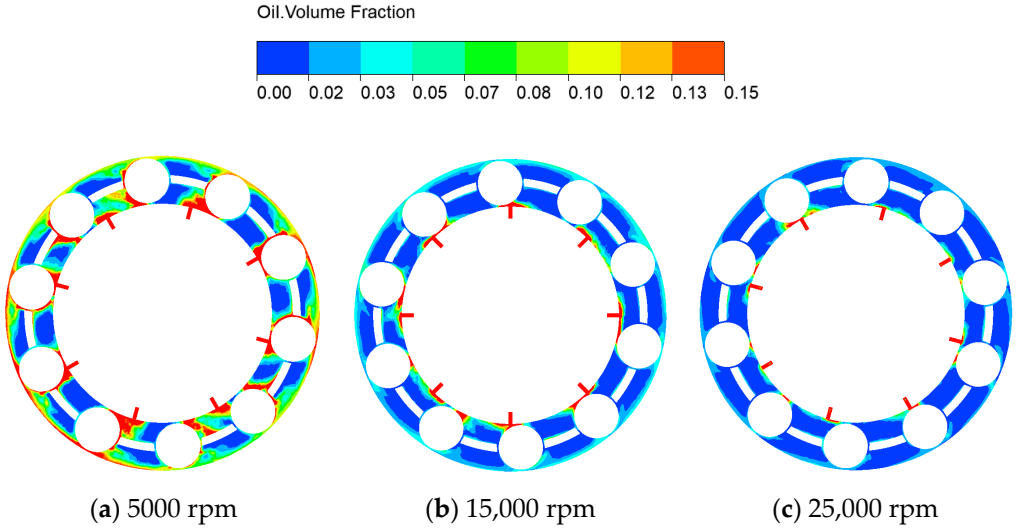
(**a**) (**b**)

Figure 6. Oil distribution within bearings at different chambers: (**a**) left chamber; (**b**) right chamber.

3.2. The Effect of Parameters on Oil Distribution

3.2.1. Bearing Rotational Speeds

Figure 7 presents the oil distribution contour maps within the bearing under different rotational speeds, based on an oil supply rate of 0.08 kg/s. The bearing configuration features under-race holes with a diameter of 1 mm, arranged in a single row of eight holes, with a double-sided oil supply configuration. The results demonstrate that oil primarily accumulates near the outer ring and in the vicinity of the inner ring oil supply holes. An increase in rotational speed leads to a gradual decrease in oil distribution observed throughout the bearing interior. This effect manifests more pronouncedly near the outer ring, where the oil transitions from a uniform to a discontinuous distribution pattern. Oil distribution near the inner ring exhibits a similar decreasing trend with increasing rotational speed.



(**a**) 5000 rpm (**b**) 15,000 rpm (**c**) 25,000 rpm

Figure 7. Oil distribution within bearings at different rotational speeds.

Figure 8 illustrates the average oil volume fraction on the raceway surfaces of the bearing inner and outer rings at different rotational speeds. An increase in rotational speed leads to a diminishing oil volume fraction on both raceways, with the rate of decrease progressively tapering off. When the rotational speed rises from 5000 rpm to 15,000 rpm, the oil volume fraction on the outer raceway decreases by 61.9%, compared to a 23.3% reduction on the inner raceway. This indicates a significantly greater reduction for the outer raceway than for the inner raceway. The underlying mechanism involves the centrifugal dynamics of oil flow: After being discharged from the supply holes, oil initially adheres to the inner raceway surface. Centrifugal forces then propel this oil away from the inner ring, and the ejected oil collides with the cage and balls. While most oil is directly expelled through the bearing cavity, a small portion penetrates through the clearances between the cage pockets and balls to reach the vicinity of the outer ring, subsequently adhering to the outer raceway surface. At higher rotational speeds, two effects intensify: greater volumes of oil are ejected from the inner ring, and the ejected oil experiences more violent collisions with the high-speed cage and rolling elements within the bearing cavity. Consequently, oil penetration through the cage pocket clearances diminishes substantially, leading to increased expulsion of oil from the bearing cavity. This results in a disproportionately severe reduction in oil volume fraction on the outer raceway. Hence, under high-speed operating conditions, increasing oil supply is necessary to ensure adequate lubrication and cooling performance.

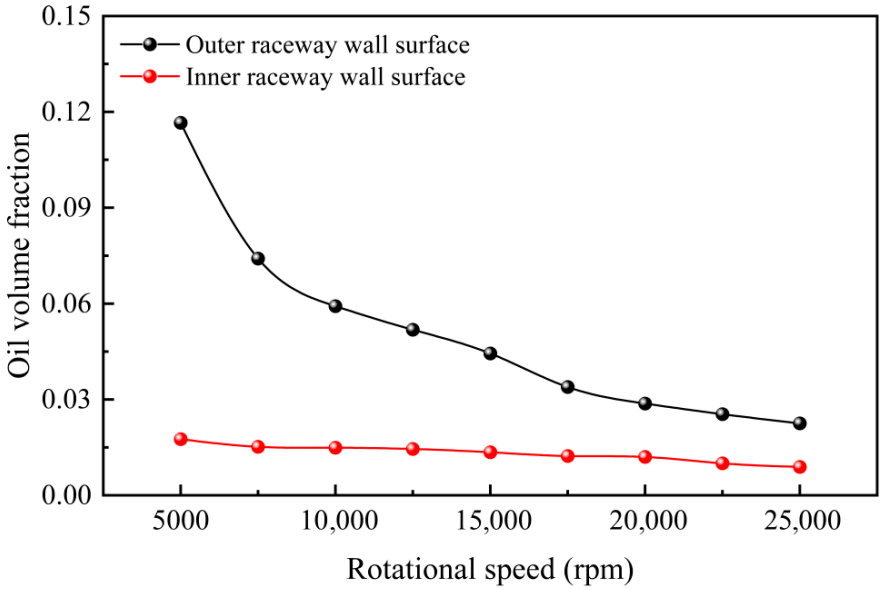
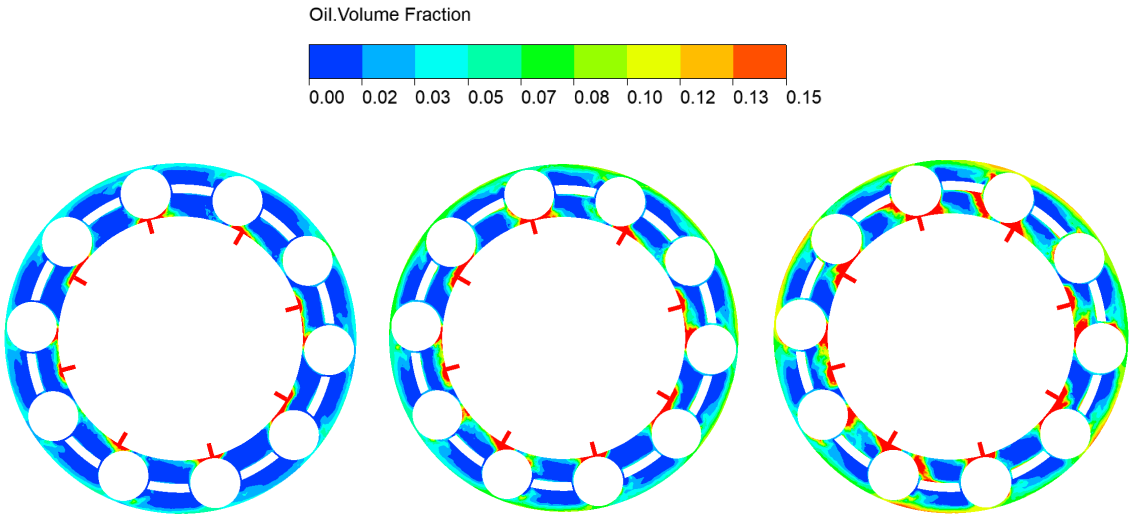


Figure 8. Oil volume fraction on inner and outer raceway walls at different bearing rotational speeds.

3.2.2. Oil Supply Rate

Figure 9 presents the oil distribution contour maps within the bearing under different oil supply rates at a constant inner ring rotational speed of 10,000 rpm. The results demonstrate that increasing the oil supply rate increases the oil volume fraction throughout the bearing interior, while causing significant accumulation occurring the outer ring. Higher oil supply rates cause greater radial velocity of the oil, enhancing its ability to penetrate through the clearances between cage pockets and balls under centrifugal forces, thereby facilitating oil migration toward the outer ring vicinity. Figure 10 displays the average oil volume fraction on the raceway surfaces of the inner and outer rings under varying oil supply rates. Both raceways exhibit increased oil volume fractions with higher supply rates, though the outer raceway shows a substantially more rapid enhancement. While the inner raceway follows a similar trend, its oil volume fraction exhibits a less pronounced increase with marginal observable change.



(**a**) 0.04 kg/s (**b**) 0.1 kg/s (**c**) 1.6 kg/s

Figure 9. Oil distribution within bearings at different oil supply rates.

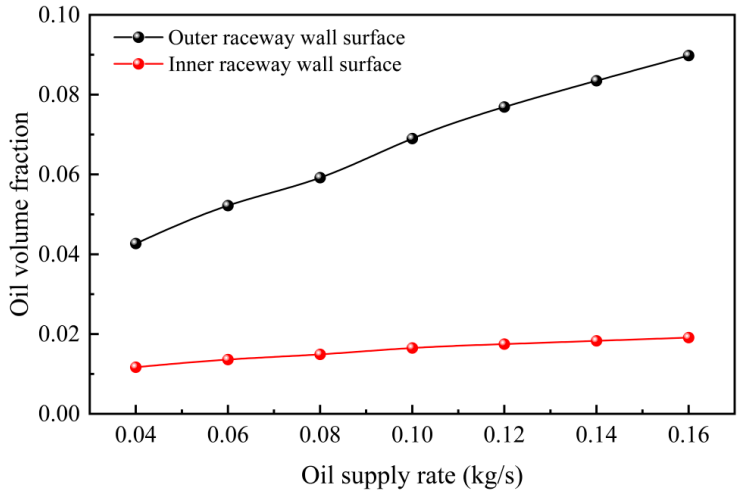


Figure 10. Oil volume fraction on inner and outer raceway walls at different oil supply rates.

3.2.3. Self-Rotation of Balls

During operation of ball bearings, the balls exhibit both orbital revolution and self-rotation. Self-rotation inherently influences the oil flow characteristics within the bearing cavity. To investigate this effect, Figure 11 compares the circumferential oil volume fraction distribution with and without the self-rotation of balls under operating conditions of 10,000 rpm inner ring speed and 0.08 kg/s oil supply rate. Results reveal a periodic circumferential oil distribution pattern corresponding precisely to the number of under-race oil supply holes. Proximal to the oil supply holes, oil volume fraction exhibits significantly higher values, whereas distal regions demonstrate a marked decline in concentration. In general, cases considering self-rotation of balls tend to overestimate the oil volume fraction. Specifically, self-rotation of balls reduces the average oil volume fraction by 20.5%, while amplifying peak-to-valley differences in the circumferential distribution by approximately 57.7% compared to the cases without considering the self-rotation of balls. This phenomenon stems from two spin-induced effects: complex flow disturbances within the cavity that disrupt oil transport pathways, and intensified oil–ball collisions accelerating centrifugal expulsion from the cavity. Simulation data shows the maximum circumferential oil fraction decreases from 0.0237 to 0.0205 when self-rotation is considered, while the minimum value drops from 0.0180 to 0.0115. These findings confirm that the self-rotation of balls significantly alters air–oil two-phase flow behavior in bearing cavities.

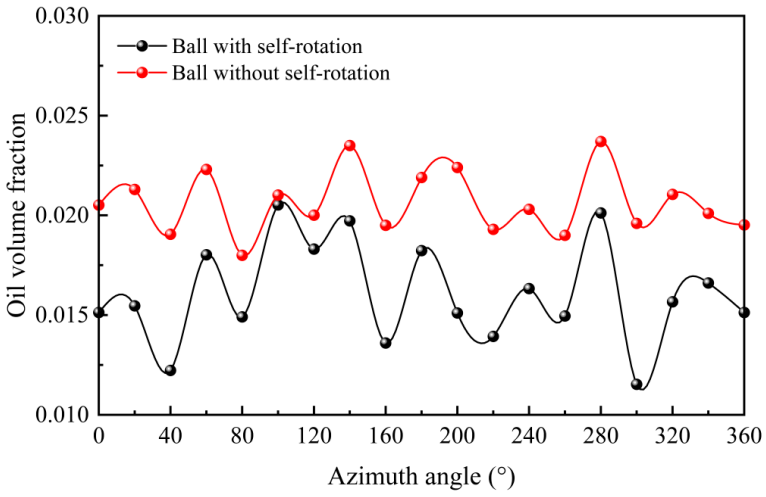


Figure 11. Oil volume fraction around the circumference of the bearing cavity.

Figure 12 illustrates the average oil volume fraction on the inner and outer raceway surfaces of the bearing when considering and neglecting self-rotation of balls under different rotational speeds. It is evident that under low-speed conditions, the outer raceway experiences a significant decrease in oil volume fraction due to the influence of self-rotation of balls, while the inner raceway exhibits an increase. However, the impact of self-rotation of balls diminishes with higher rotational speeds. This phenomenon indicates that the self-rotation effect of balls acts as a critical regulatory factor in oil distribution under low-speed operating conditions. The oil migration pattern induced by this effect directly determines the quality of lubrication performance under such conditions, which provides important guidance for the lubrication design of low-speed bearings. When self-rotation of balls is considered, the volume fraction on the inner raceway surface exceeds that on the outer raceway—an inverse trend to observations made when neglecting the self-rotation of balls. This phenomenon is further validated by the oil distribution contour maps shown in Figures 13–15 for the raceway surfaces and bearing cavity cross-sections. With self-rotation of balls, oil flung from the inner ring collides more violently with the balls, becoming atomized into oil droplets. Self-rotation of balls propels most of this oil mist toward regions adjacent to the inner ring, consequently increasing oil distribution near the inner race, as illustrated in Figure 15; this results in a higher oil volume fraction on the inner raceway surface (Figure 13). Conversely, with the influence of self-rotation of balls, the volume of oil flowing from the clearance between the cage pocket and the ball to the outer race is thus reduced. Consequently, the oil volume fraction on the outer raceway surface significantly decreases, as demonstrated in Figure 14. This revelation of the mechanism not only deepens the understanding of the complex flow behavior of oil–air two-phase flow within the bearing but also clarifies the coupling relationship between the dynamic motion of balls and oil distribution. It provides a theoretical basis for optimizing the bearing lubrication structure. By regulating the interaction between the self-rotation of balls and oil, the lubrication uniformity under different operating conditions can be specifically enhanced.

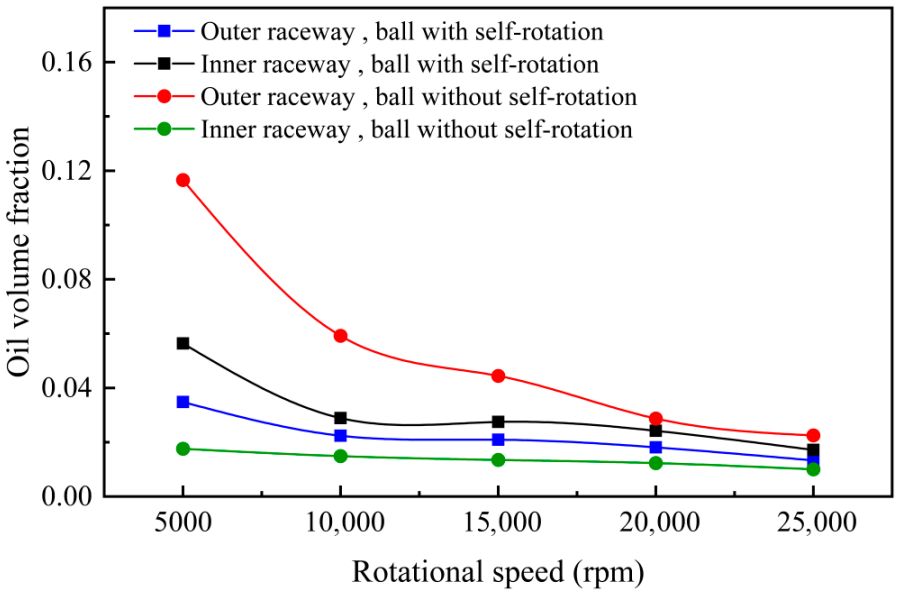


Figure 12. The influence of self-rotation of balls on oil volume fraction on inner and outer raceway walls at different bearing rotational speeds.

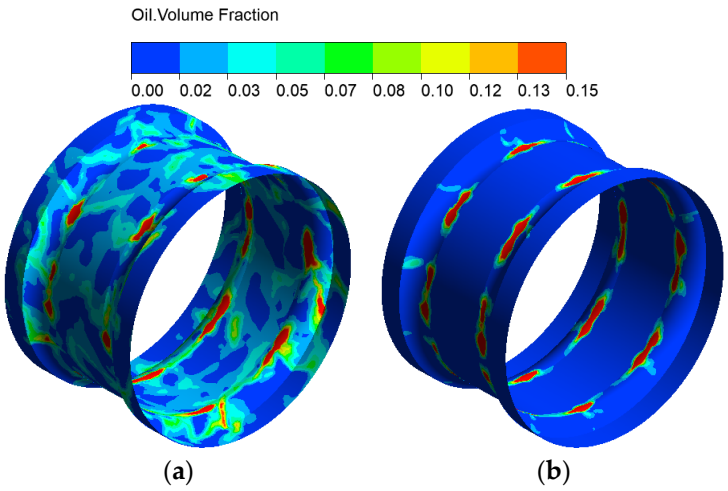


Figure 13. Oil distribution in inner ring wall surface: (**a**) case of balls with self-rotation; (**b**) case of balls without self-rotation.

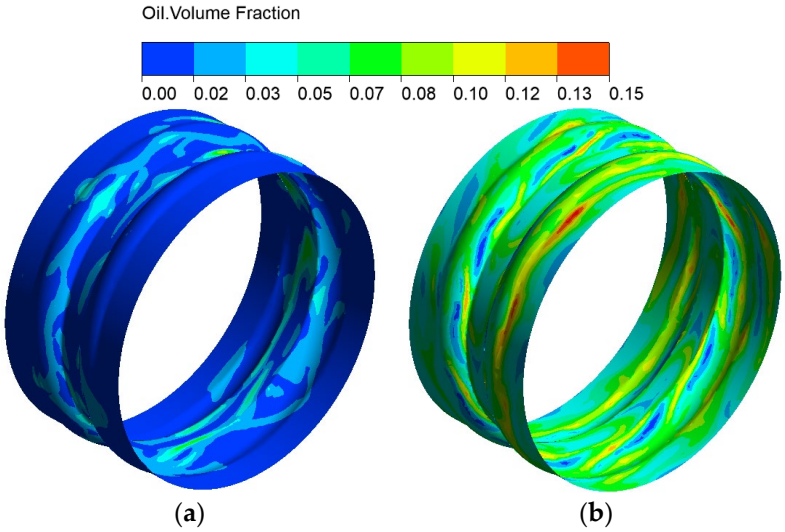


Figure 14. Oil distribution in outer ring wall surface: (**a**) case of balls with self-rotation; (**b**) case of balls without self-rotation.

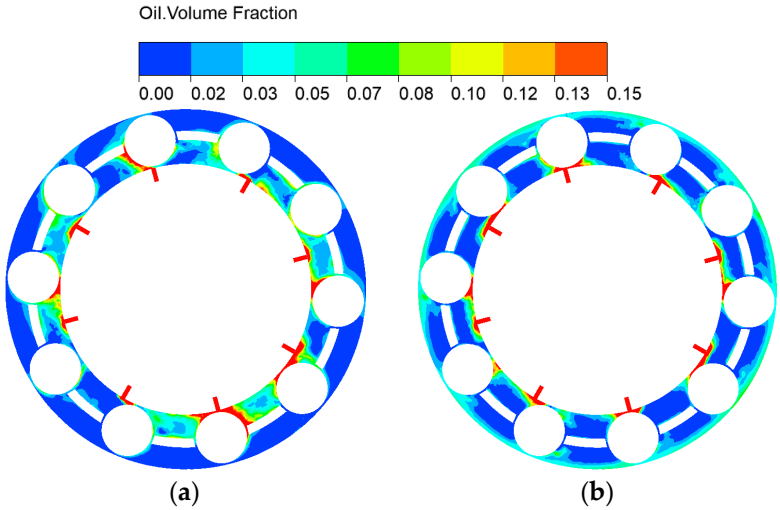


Figure 15. Oil distribution in the left chamber of the bearing: (**a**) case of balls with self-rotation; (**b**) case of balls without self-rotation.

3.2.4. Number of Under-Race Holes

To investigate the impact of under-race oil supply hole number on the oil–air two-phase flow field within bearings, simulations are conducted for five distinct hole numbers. Figure 16 displays the oil distribution contour maps within the bearing under different numbers of under-race holes, with a constant inner ring rotational speed of 10,000 rpm and a total oil supply rate of 0.08 kg/s. The results indicate that increasing the number of oil supply holes enhances oil distribution uniformity and coverage throughout the bearing interior, notably across the outer raceway. With merely two under-race holes per side chamber, oil accumulates near the inner ring oil supply holes, while distribution on the outer raceway becomes asymmetric-concentrated on one side but sparse on the opposite. As the number of under-race holes increases to ten, however, the outer raceway exhibits uniform oil coverage, and no significant accumulation near the inner ring is observed. Figure 17 illustrates the average oil volume fraction on the inner and outer raceway surfaces under varying numbers of under-race holes. As hole number rises, oil volume fractions increase across both raceways, though the outer raceway exhibits a more pronounced increasing trend, which is attributed to the greater number of holes enhancing oil flow toward the outer ring region via the clearance between the cage pocket and balls.

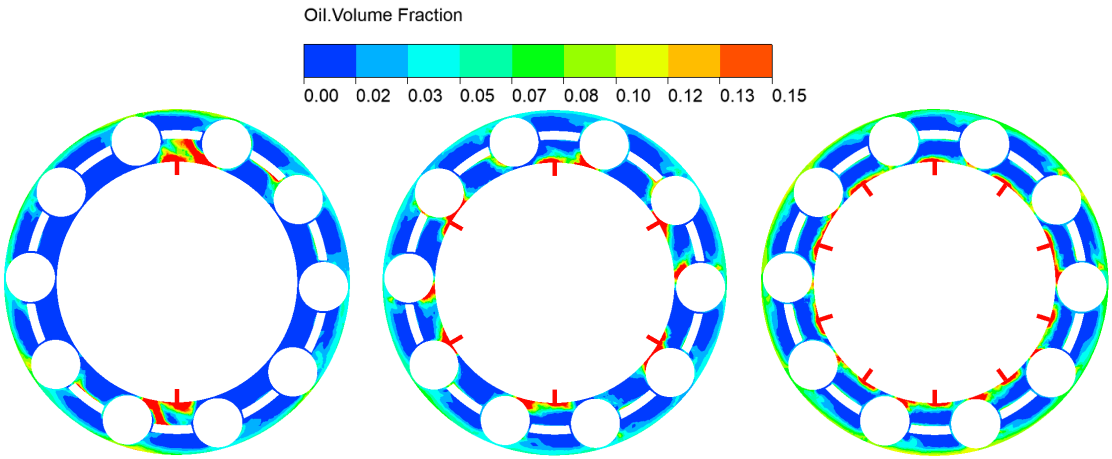


Figure 16. Oil distribution within bearings at different numbers of under-race oil supply holes.

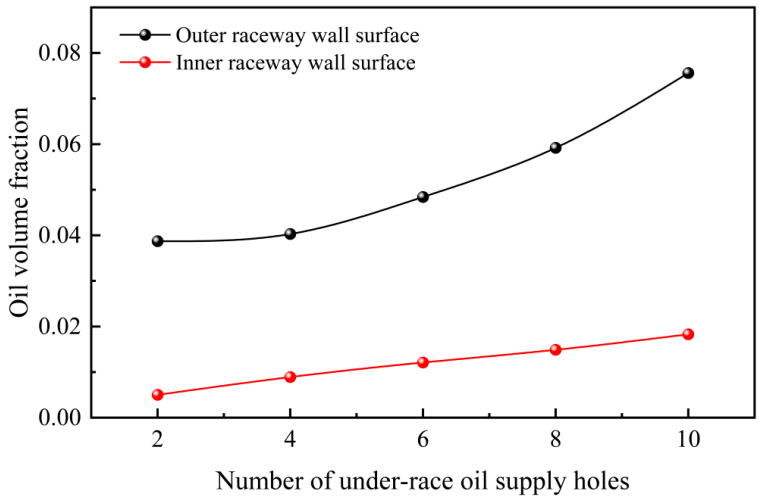
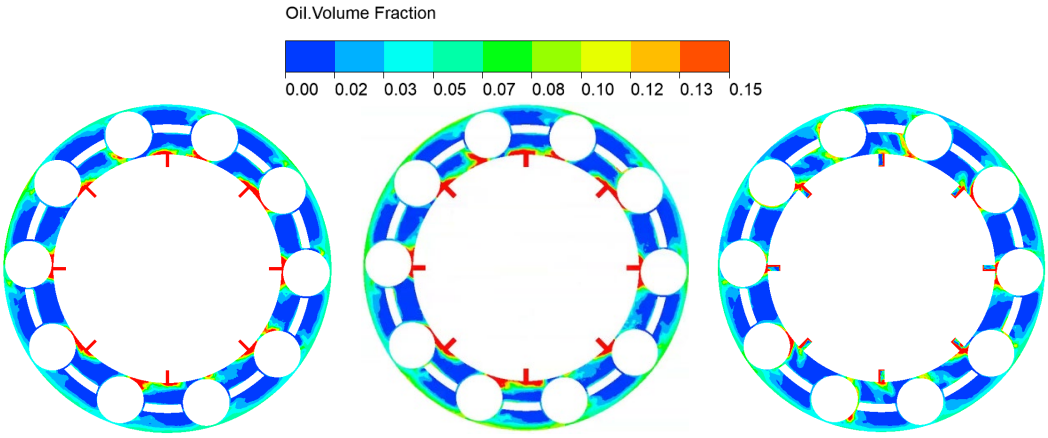


Figure 17. Oil volume fraction on inner and outer raceway walls at different numbers of under-race oil supply holes.

3.2.5. Diameter of Under-Race Holes

To investigate the influence of under-race oil supply hole diameter on the oil–air two-phase flow field within bearings, simulations are performed for five distinct hole diameters. Figure 18 presents the oil distribution contour maps inside the bearing for different under-race hole diameters, with a constant inner ring rotational speed of 10,000 rpm and a total oil supply rate of 0.08 kg/s. The results indicate that as the hole diameter increases from 0.8 mm to 1.2 mm, oil distribution within the bearing cavity increases. Conversely, when the diameter expands from 1.2 mm to 1.6 mm, the oil distribution decreases. This nonlinear behavior occurs because increased hole diameters intensify fluid–structure impacts, enhancing interactions between balls and oil. Consequently, more oil is ejected outward from the bearing cavity, reducing overall oil retention. Figure 19 displays the average oil volume fractions on the inner and outer raceway surfaces with different under-race hole diameters. The graph reveals that as the hole diameter increases, oil volume fractions on both raceway surfaces initially rise and then decline. Maximum oil volume fractions occur at a diameter of 1.2 mm for both raceways. This conclusion directly provides a basis for optimizing the diameter of oil supply holes and also offers theoretical support for "avoiding excessive enlargement of hole diameter" in lubrication structure design.



(**a**) 0.8 mm (**b**) 1.2 mm (**c**) 1.6 mm

Figure 18. Oil distribution within bearings at different diameters of under-race oil supply holes.

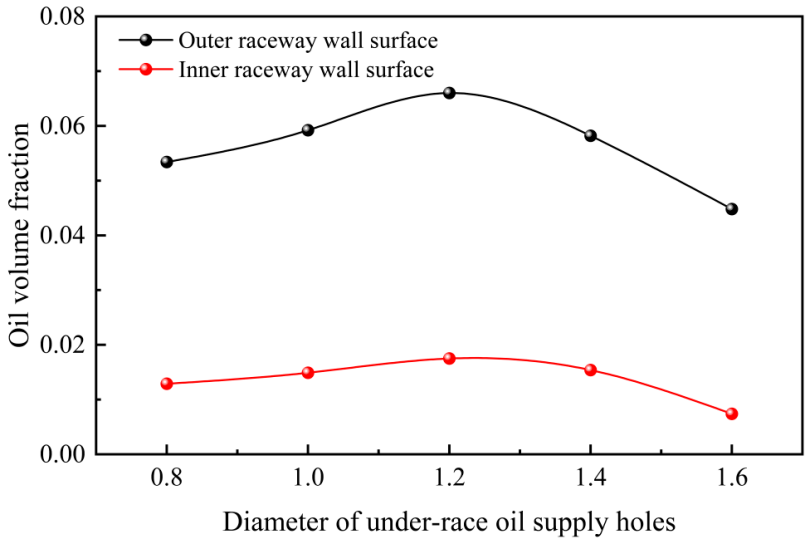


Figure 19. Oil volume fraction on inner and outer raceway walls at different diameters of under-race oil supply holes.

3.2.6. Axial Position of Under-Race Holes

In addition to the number and diameter of under-race holes, their position also significantly impacts the two-phase flow field within the bearing cavity. For the lubrication of double-row tapered roller bearings, oil supply holes are typically drilled in the middle of the outer ring [21]. Therefore, considering the structural features of the double-row ball bearing's inner ring and the characteristics of under-race lubrication, a single-sided oil supply configuration was adopted, which positioned under-race holes at the inner ring's mid-section. Compared to the double-sided oil supply configuration, this single-sided configuration requires fewer holes, simplifying manufacturing processes and enabling hole placement away from the contact zone (stress concentration areas), thereby avoiding structural weakening. However, its lubrication effectiveness remained unclear. To evaluate the lubrication performance of this single-sided design, simulations were conducted, and results are compared with those by double-sided oil supply configuration. Figure 20 illustrates the oil volume fraction distribution along the bearing cavity's circumferential direction for different lubrication configurations, with an inner ring rotational speed of 10,000 rpm and an oil supply rate of 0.08 kg/s. The results indicate that single-sided lubrication yields a significantly lower circumferential oil volume fraction than double-sided oil supply configuration—a reduction of 52.3% within the cavity. This substantial decline in lubrication effectiveness is further corroborated by Figures 21–23. Under single-sided oil supply configuration, oil emerging from the mid-section under-race holes passes directly through the center between the two cages under centrifugal force; subsequently, oil reaches the outer ring region before being discharged from the bearing cavity, as depicted in Figure 21b. Consequently, the oil does not directly collide with the balls. Additionally, centrifugal forces impede oil flow back from the outer ring region to the inner raceway surface through the cage pocket–ball clearance. As shown in Figure 22b, this results in negligible oil distribution on the inner raceway surface. This leads to the heat in the contact area between the inner raceway and the balls failing to dissipate in time, causing the temperature in this region to continuously rise. Meanwhile, it may result in uneven thermal expansion of the cage, which in turn triggers seizing between the cage and the balls, ultimately leading to bearing failure. Furthermore, oil distribution on the outer raceway surface exhibits greater non-uniformity under single-sided oil supply configuration than under double-sided oil supply configuration. As presented in Figure 23, the average oil volume fraction decreases by 27%, indicating a moderate decline in lubrication effectiveness. From this, it follows that although single-sided oil supply configuration offers advantages in processing convenience and structural strength, its single oil supply path severely restricts oil coverage and uniformity—with lubrication blind spots particularly prone to form on the inner raceway surface. This finding provides a reference for designing under-race lubrication structures in double-row ball bearings: in high-reliability lubrication scenarios, double-sided oil supply configuration should be prioritized; when single-sided oil supply configuration is necessary due to processing constraints, targeted optimization of oil hole positions or auxiliary structures is required to enhance lubrication performance.

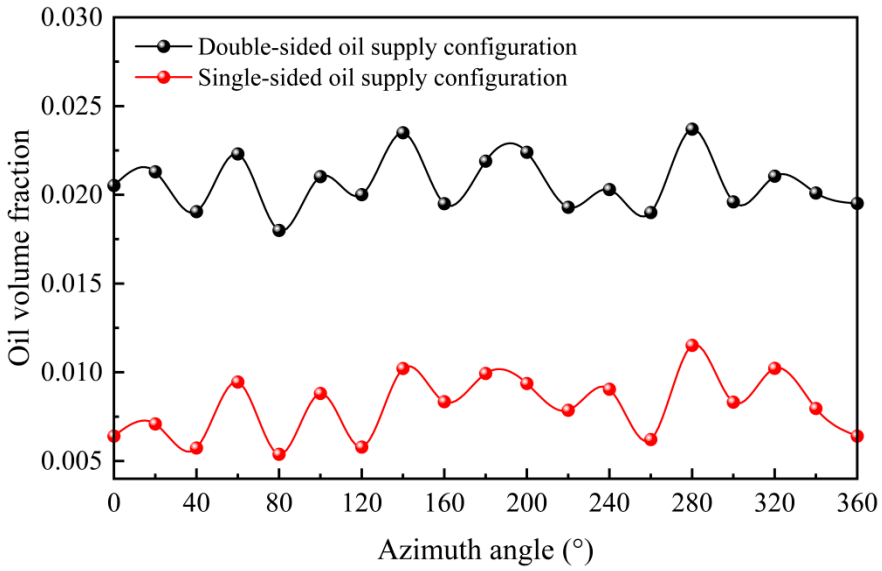


Figure 20. Oil volume fraction around the circumference of the bearing cavity at different oil supply configurations.

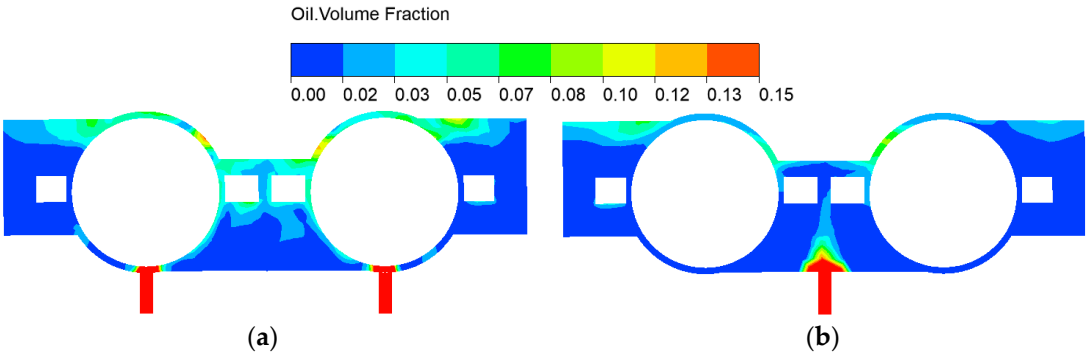


Figure 21. Oil distribution at different oil supply configurations: (**a**) double-sided oil supply configuration; (**b**) single-sided oil supply configuration.

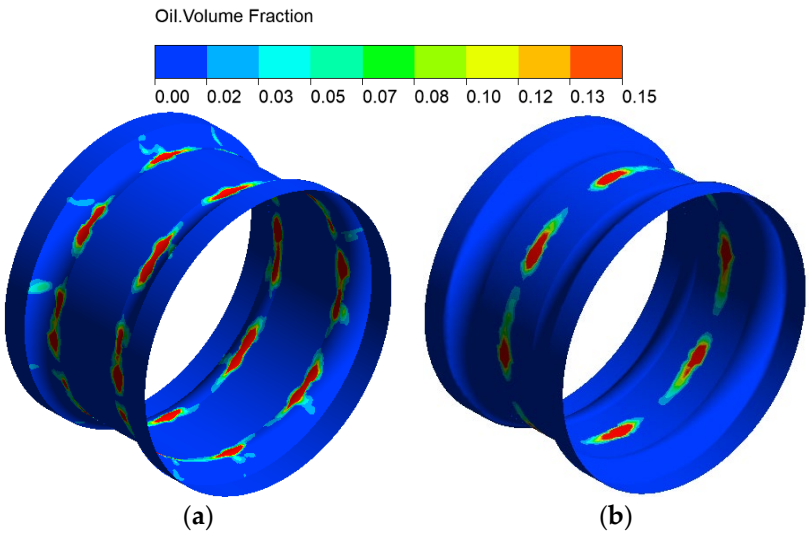


Figure 22. Oil distribution in inner ring wall surface at different oil supply configurations: (**a**) double-sided oil supply configuration; (**b**) single-sided oil supply configuration.

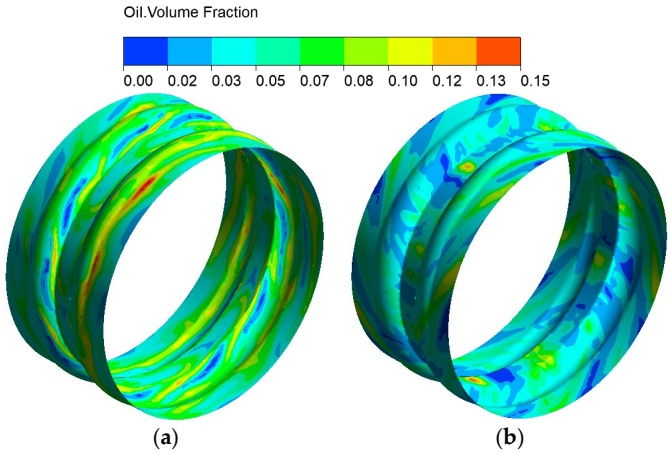


Figure 23. Oil distribution in outer ring wall surface at different oil supply configurations: (**a**) double-sided oil supply configuration; (**b**) single-sided oil supply configuration.

3.2.7. Circumferential Position of Under-Race Hole

To investigate the influence of the circumferential position of under-race holes on the two-phase flow field in the bearing cavity, simulations were conducted for the asymmetric distribution of under-race holes. Specifically, the under-race holes on the left and right sides of the double-row ball bearing differ by 22.5° in circumferential position. Figure 24 shows the oil volume fraction around the circumference of the bearing cavity under different circumferential positions of the under-race holes, with an inner ring rotational speed of 10,000 rpm and an oil supply rate of 0.08 kg/s. The results indicate that the circumferential distribution pattern of the oil remains largely unchanged under the asymmetric distribution of under-race holes. Compared with the symmetric distribution of under-race holes, the oil volume fraction only increases slightly. Figure 25 presents the contour maps of oil distribution in the cross-sections of the left and right chambers of the double-row ball bearing under the asymmetric distribution of under-race holes. It can be observed that the oil distribution in the outer ring regions of both chambers is generally consistent, with no significant changes resulting from the differing circumferential positions of the under-race holes on either side. However, the oil distribution in the inner ring regions of the two chambers does vary due to the differing circumferential positions of the under-race holes. This indicates that the circumferential position of under-race holes has a minor overall impact on the two-phase flow field in the bearing cavity; thus, this factor can be neglected in the subsequent optimization of bearing lubrication structures.

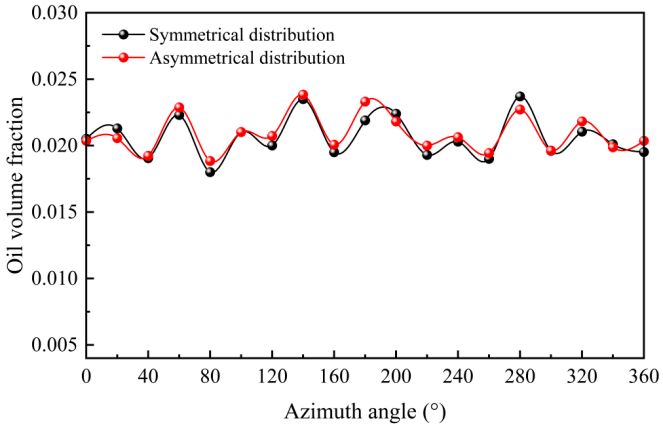
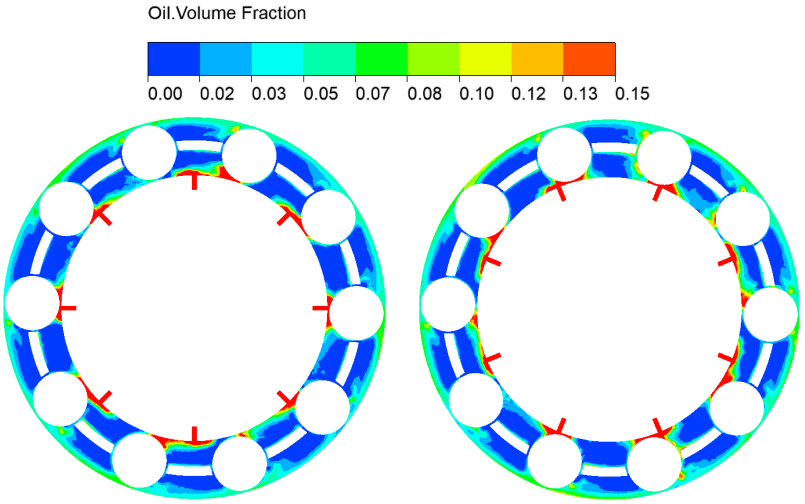


Figure 24. Oil volume fraction around the circumference of the bearing cavity under different circumferential position of under-race hole.

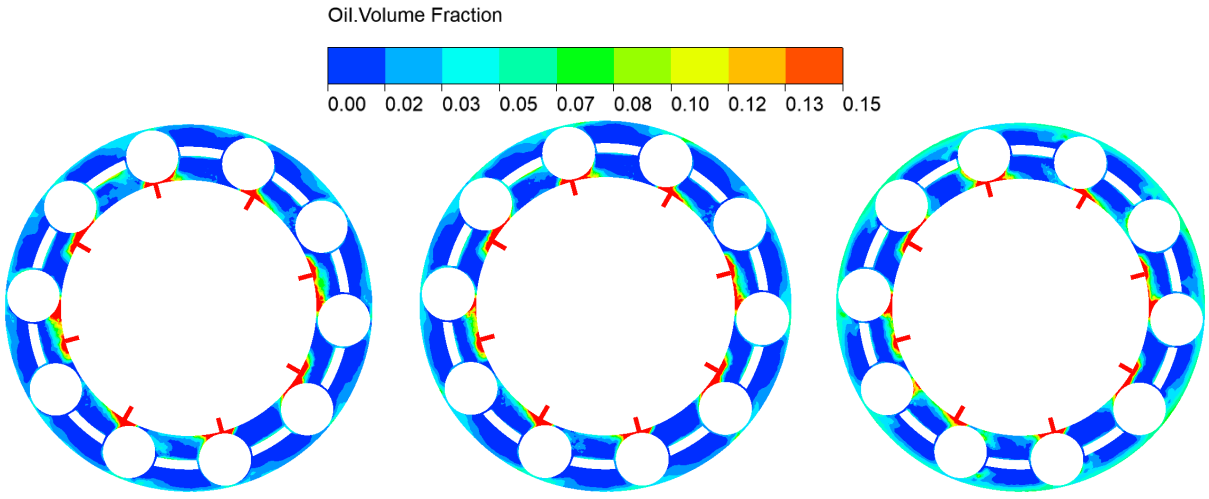


(**a**) Left side (**b**) Right side

Figure 25. Oil distribution at different cavities under asymmetrical distribution of under-race holes.

3.2.8. Oil Viscosity

The flow characteristics of oil within bearing cavities are influenced not only by operational parameters and structural design but also by its own physicochemical properties, such as viscosity. Figure 26 presents the contour maps of oil distribution inside the bearing for different oil viscosities, tested under a constant inner ring rotational speed of 10,000 rpm, oil supply rate of 0.08 kg/s, and oil density of 970 kg/m^3. The results reveal that increasing oil viscosity expands cavity oil distribution and distributes oil more uniformly near the outer race. Circumferential oil concentration within the bearing further rises under higher viscosity conditions, as illustrated in Figure 27. Contrastingly, viscosity demonstrates secondary influence on cavity oil distribution when compared to the prominent effects of rotational speed and oil supply rate. While higher viscosity improves lubrication effectiveness, it concurrently increases fluid viscous dissipation. Consequently, selecting an optimal oil viscosity is essential to balance lubrication efficacy and energy efficiency in operational contexts.



(**a**) 0.0039 Pa·s (**b**) 0.0114 Pa·s (**c**) 0.0318 Pa·s

Figure 26. Oil distribution within bearings at different oil viscosities.

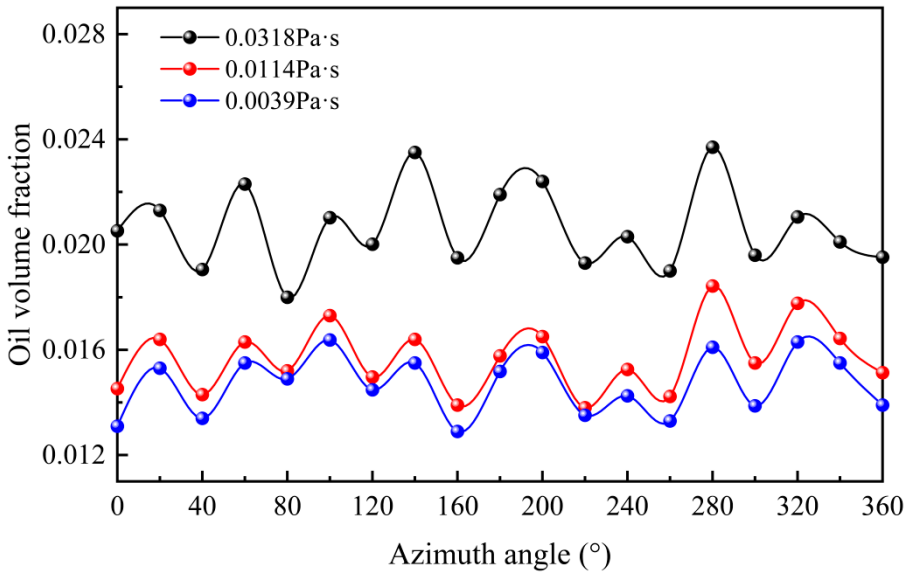


Figure 27. Oil volume fraction around the circumference of the bearing cavity at different oil viscosities.

3.2.9. Oil Density

During bearing operation, oil density varies with temperature and pressure. Figure 28 displays the oil distribution contour maps inside the bearing cavity under different oil densities, with a constant inner ring rotational speed of 10,000 rpm, oil supply rate of 0.08 kg/s, and oil viscosity of 0.0318 Pa·s. Increased oil density produces negligible alteration in bearing cavity oil distribution pattern. The spatial distribution pattern and periodic variation in oil along the bearing cavity's circumference persist consistently, though the oil volume fraction exhibits a slight decrease with increasing density, as illustrated in Figure 29. This minor reduction occurs because higher-density oil experiences greater centrifugal forces, promoting its ejection outward from the bearing cavity. Notably, compared to the substantial impacts of bearing rotational speed, oil supply rate, and viscosity on oil distribution, the influence of density is relatively negligible.

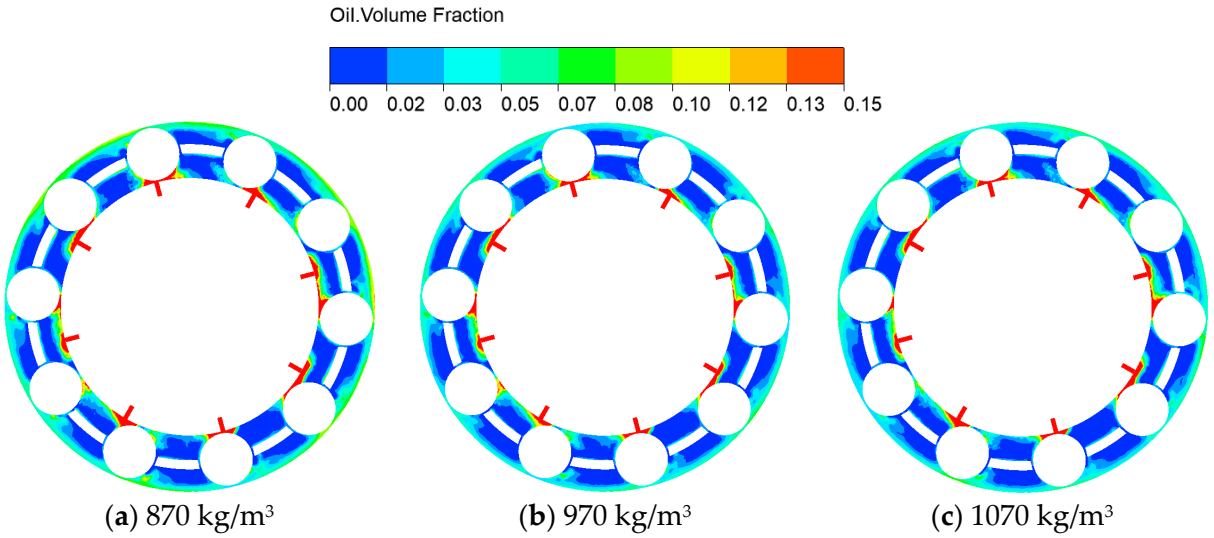


Figure 28. Oil distribution within bearings at different oil densities.

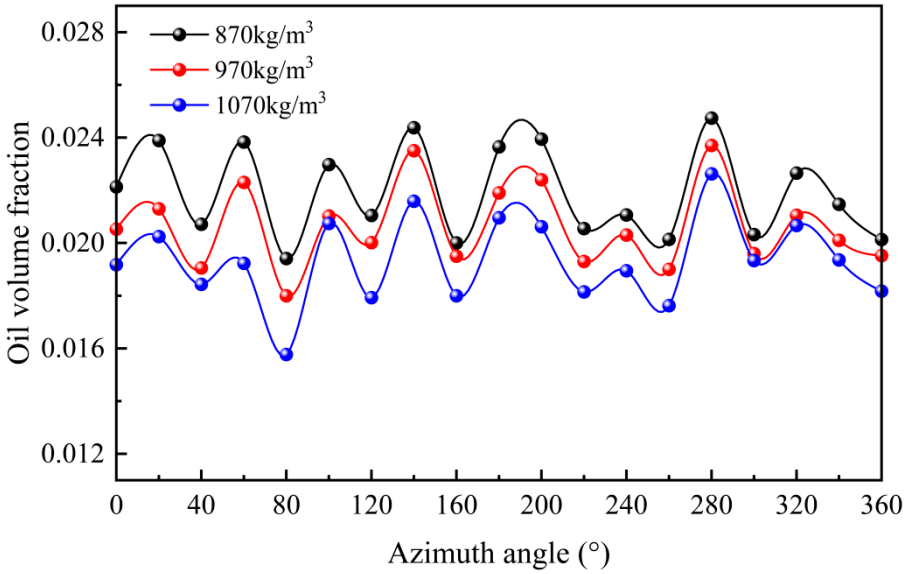


Figure 29. Oil volume fraction around the circumference of the bearing cavity at different oil densities.

4. Conclusions

By establishing a numerical simulation model for an under-race lubricated double-row ball bearing, this study systematically investigated the influence patterns of multiple parameters—including inner ring rotational speed, oil supply rate, self-rotation of balls, number of under-race holes, diameter of oil supply holes, lubrication configuration, oil viscosity, and density—on the distribution of oil–air two-phase flow within the bearing and the average volume fraction of oil on the inner and outer race surfaces. The core conclusions are summarized as follows:

(1) The oil distribution inside the bearing is dominated by centrifugal force, exhibiting asymmetric characteristics with oil enrichment at the outer ring and depletion at the inner ring (the average volume fraction on the outer ring surface is significantly higher than that on the inner ring). Circumferential oil distribution exhibits periodic variations synchronized with the number of under-race holes. Additionally, oil concentration is higher near the under-race holes and lower in regions farther away from them.

(2) Increasing inner ring rotational speed reduces the oil volume fraction on both raceway surfaces, while higher oil supply rates increase it. Among these, oil supply rate is the key parameter directly determining the total oil supply quantity, while rotational speed affects the distribution pattern by indirectly regulating the migration direction of the oil. An increase in oil viscosity can elevate the overall oil volume fraction within the bearing cavity (suppressing oil flow dispersion), making it a critical physical property parameter for adjusting lubrication performance. In contrast, although an increase in oil density leads to a decrease in the oil volume fraction, the effect is insignificant, thus it can be considered an auxiliary parameter.

(3) The self-rotation of balls reduces the overall oil volume fraction within the bearing cavity, causing a substantial decrease in the outer raceway's oil volume fraction while markedly increasing that of the inner raceway. The self-rotation effect is particularly prominent at low rotational speeds, whereas it becomes negligible at high rotational speeds. This indicates that the self-rotation of balls is a critical factor requiring special attention under low-speed operating conditions, and its coupling effect with rotational speed directly determines the lubrication performance.

(4) Compared with single-sided oil supply structures, double-sided oil supply structures exhibit higher circumferential oil volume fractions. Changes in the circumferential position of under-race holes do not alter the overall oil distribution within the bearing cavity. Increasing the number of under-race holes simultaneously enhances the oil volume fractions on both the inner and outer ring surfaces. However, the influence of oil supply hole diameter on the volume fraction follows a "first-increase-then-decrease" trend, with an optimal diameter existing. Therefore, synergistic optimization of the oil supply structure and parameters (number and diameter) is required in under-race lubrication design to improve lubrication uniformity.

This study systematically analyzes and identifies the key influencing factors and action mechanisms of the oil–air two-phase flow in under-race lubricated double-row ball bearings, providing a theoretical basis for bearing lubrication design. However, current research has not accounted for thermal effects and interactions between parameters. Thus, future studies will conduct heat generation calculations and heat transfer coupling research to reveal the interaction between the temperature field and lubrication field, aiming to improve lubrication design.

Author Contributions: Conceptualization, X.H. and J.L.; methodology, X.H. and J.L.; software, J.L.; validation, J.L.; writing—original draft preparation, J.L.; writing—review and editing, X.H. and J.L.; visualization, J.L.; project administration, X.H.; funding acquisition, X.H. All authors have read and agreed to the published version of the manuscript.

Funding: This research was funded by the science and technology innovation Program of Hunan Province(2024RC1001), and the National Natural Science Foundation of China (52475078).

Data Availability Statement: The original contributions presented in this study are included in the article. Further inquiries can be directed to the corresponding author.

Conflicts of Interest: The authors declare no conflicts of interest.

References

1. Jiang, L.; Liu, Z.X.; Huang, W.A.; Lyu, Y.; Li, Y.J.; Hou, Y.K.; Liu, Y.W. Numerical and experimental investigation on two-phase flow and oil capture efficiency of under-race lubrication for high-speed bearings. *Phys. Fluids* **2024**, *36*, 063336. [CrossRef]
2. Gloeckner, P.; Rodway, C. The Evolution of Reliability and Efficiency of Aerospace Bearing Systems. *Engineering* **2017**, *9*, 962–991. [CrossRef]
3. Gloeckner, P.; Dullenkopf, K.; Flouros, M. Direct Outer Ring Cooling of a High Speed Jet Engine Mainshaft Ball Bearing: Experimental Investigation Results. *J. Eng. Gas Turbines Power-Trans. Asme* **2011**, *133*, 062503. [CrossRef]
4. Hu, J.; Wu, W.; Wu, M.; Yuan, S. Numerical investigation of the air–oil two-phase flow inside an oil-jet lubricated ball bearing. *Int. J. Heat Mass Transf.* **2014**, *68*, 85–93. [CrossRef]
5. Pang, B.T.; Li, J.S.; Liu, H.B.; Ma, W.; Xue, Y.J. A simulation study on optimal oil spraying mode for high-speed rolling bearing. *J. Achiev. Mater. Manuf. Eng.* **2008**, *31*, 553–557.
6. Jiang, L.; Liu, Z.X.; Lyu, Y.G.; Qin, J.W. Numerical simulation on the oil capture performance of the oil scoop in the under-race lubrication system. *Proc. Inst. Mech. Eng. Part G-J. Aerosp. Eng.* **2021**, *235*, 2258–2273. [CrossRef]
7. Cavallaro, G.; Nelias, D.; Bon, F. Analysis of High-Speed Intershaft Cylindrical Roller Bearing with Flexible Rings. *Tribol. Trans.* **2005**, *48*, 154–164. [CrossRef]
8. Peterson, W.; Russell, T.; Sadeghi, F.; Berhan, M.T.; Stacke, L.E.; Ståhl, J. A CFD investigation of lubricant flow in deep groove ball bearings. *Tribol. Int.* **2021**, *154*, 106735. [CrossRef]
9. Wu, W.; Hu, J.; Yuan, S.; Hu, C. Numerical and experimental investigation of the stratified air-oil flow inside ball bearings. *Int. J. Heat Mass Transf.* **2016**, *103*, 619–626. [CrossRef]
10. Yan, K.; Wang, Y.; Zhu, Y.; Hong, J. Investigation on the effect of sealing condition on the internal flow pattern of high-speed ball bearing. *Tribol. Int.* **2017**, *105*, 85–93. [CrossRef]
11. Qian, S.K.; Wang, B.M.; Du, X.B.; Chen, X. Lubrication enhancement of high-speed angular contact ball bearings by adding diversion hole in cage. *J. Braz. Soc. Mech. Sci. Eng.* **2025**, *47*, 164. [CrossRef]

12. Dai, Y.; Tang, R.Q.; Yu, C.; Yang, C.H.; Yang, D.; Zhu, X. Air-oil two-phase flow and oil penetration characteristics of angular contact ball bearing under oil jet lubrication: Numerical and experimental investigations. *Phys. Fluids* **2025**, *37*, 047133. [CrossRef]
13. Adeniyi, A.A.; Morvan, H.; Simmons, K. A computational fluid dynamics simulation of oil-air flow between the cage and inner race of an aero-engine bearing. *J. Eng. Gas Turbines Power* **2017**, *139*, 012506. [CrossRef]
14. Gao, W.J.; Nelias, D.; Li, K.; Liu, Z.X.; Lyu, Y.G. A multiphase computational study of oil distribution inside roller bearings with under-race lubrication. *Tribol. Int.* **2019**, *140*, 105862. [CrossRef]
15. Adeniyi, A.; Morvan, H.; Simmons, K. A multiphase computational study of oil-air flow within the bearing sector of Aeroengines. In Proceedings of the ASME Turbo Expo 2015: Turbine Technical Conference and Exposition, Montreal, QC, Canada, 15–19 June 2015. [CrossRef]
16. Yu, Q.; Gao, W.; Gong, P.; Li, Y.; Li, C. Oil Distribution around Ball-Raceway Local Contact Region in Under-Race Lubrication of Ball Bearing. *Dynamics* **2024**, *4*, 731–746. [CrossRef]
17. Gong, P.; Liu, Z.X.; Yu, Q.J.; Chen, F. Research on internal two-phase flow in the local micro-clearance design of a high-speed ball bearing with under-race lubrication. *Lubr. Sci.* **2024**, *36*, 216–230. [CrossRef]
18. Wei, C.H.; Wu, W.; Li, T.; Massi, F.; Zhao, J. Experimental and Simulation Analysis of oil-air Two-Phase Flow Characteristics in High-Speed Bearings. *Tribol. Int.* **2025**, *201*, 110281. [CrossRef]
19. Bao, H.; Hou, X.; Tang, X.; Lu, F. Analysis of temperature field and convection heat transfer of oil-air two-phase flow for ball bearing with under-race lubrication. *Ind. Lubr. Tribol.* **2021**, *73*, 817–821. [CrossRef]
20. Bao, H.Y.; Wang, C.L.; Lu, F.X. Temperature impact analysis of star gear bearing inner ring based on under-race lubrication passage. *J. Mech. Sci. Technol.* **2020**, *34*, 5271–5278. [CrossRef]
21. Zhu, W.; Zhu, R.; Tang, X.; Lu, F.; Bai, X.; Wu, X.; Li, F. CFD-Based Analysis of Oil and Gas Two-Phase Flow Characteristics in Double-Row Tapered Roller Bearings with Different Rib Structures. *Appl. Sci.* **2022**, *12*, 1156. [CrossRef]
22. Bai, X.; Lu, F.; Zhu, Z.R. Lubricant distribution evolution in asymmetric double-row tapered roller bearings during the loss of lubrication process. *Int. J. Des. Eng. IJDE* **2023**, *12*, 49–68. [CrossRef]
23. Hirt, C.W.; Nichols, B.D. Volume of fluid (VOF) method for the dynamics of free boundaries. *J. Comput. Phys.* **1981**, *39*, 201–225. [CrossRef]
24. Shan, W.; Chen, Y.; Huang, J.; Wang, X.; Han, Z.; Wu, K. A multiphase flow study for lubrication characteristics on the internal flow pattern of ball bearing. *Results Eng.* **2023**, *20*, 101429. [CrossRef]
25. Jiang, L.; Lyu, Y.; Gao, W.; Zhu, P.; Liu, Z. Numerical investigation of the oil–air distribution inside ball bearings with under-race lubrication. *Proc. Inst. Mech. Eng. Part J J. Eng. Tribol.* **2022**, *236*, 499–513. [CrossRef]
26. Lyu, Y.; Li, Y.H.; Li, C.; Jiang, L.; Liu, Z.X. Oil-Air Distribution Prediction Inside Ball Bearing with Under-Race Lubrication Based on Numerical Simulation. *Appl. Sci.* **2024**, *14*, 3770. [CrossRef]

Disclaimer/Publisher's Note: The statements, opinions and data contained in all publications are solely those of the individual author(s) and contributor(s) and not of MDPI and/or the editor(s). MDPI and/or the editor(s) disclaim responsibility for any injury to people or property resulting from any ideas, methods, instructions or products referred to in the content.